

VESSEL CENTERLINE DETECTION IN RETINAL IMAGES BASED ON A CORNER DETECTOR AND DYNAMIC THRESHOLDING

Ivo Soares^{1,2}, Miguel Castelo-Branco¹, António M.G. Pinheiro²

¹CICS - Research Centre of Health Sciences, University of Beira Interior, Covilhã, Portugal

²Remote Sensing Unit/Optics Center, University of Beira Interior, Covilhã, Portugal

ABSTRACT

This paper describes a new method for the calculation of the retinal vessel centerlines using a scale-space approach for an increased reliability and effectiveness. The algorithm begins with a new vessel detector description method based on a modified corner detector. Then the vessel detector image is filtered with a set of binary rotating filters, resulting in enhanced vessels structures. The main vessels can be selected with a dynamic thresholding approach. In order to deal with vessels bifurcations and vessels crossovers that might not be detected, the initial retinal image is processed with a set of four directional differential operators. The resulting directional images are then combined with the detected vessels, creating the final vessels centerlines image. The performance of the algorithm is evaluated using two different datasets.

Index Terms— Vessel centerline, scale-space, Retina

1. INTRODUCTION

The larger and most predominant structure in retinal fundus images are the vessels. Morphological changes in the retinal vasculature, such as diameter, length, branching angles or tortuosity, allows the detection of diseases such as glaucoma, diabetic retinopathy, and hypertensive retinopathy (see Figure 1) [1, 2]. Hence, an automatic and reliable vessel extraction is a major prerequisite for subsequent retinal image analysis [3]. A comprehensive review in vessels segmentation was presented in [4]. Effective retinal centerline calculation has a crucial role, both as a step towards a final vessel segmentation [4, 5] or in the measure of vascular tortuosity [1, 6]. Although there is a strong attention to the retinal fundus images, few works were proposed that specifically deal with the retinal vessels centerline detection. In [3] Sofka et al. proposed a likelihood ratio test that combines matched filter responses, confidence measures and vessels boundary measures. A graph-based approach was developed by Jaydeep et al. to trace the retinal vessel trees [2]. Zana et al. [7] proposed a mathematical morphology and curvature based method for the detection of vessel-like patterns. In this paper, an efficient and reliable method that is capable of detecting the vessels centerlines in retinal images is proposed. The rest of this pa-

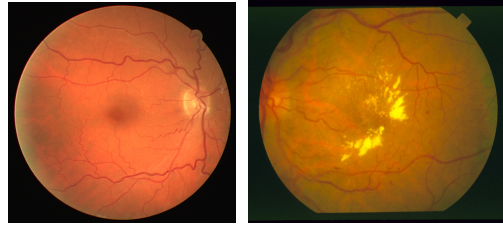


Fig. 1: Retinal fundus images with vascular tortuosity.

per is organized as follows. The proposed vessel centerline detection technique is presented in Section 2. Experimental results are described and discussed in Section 3. Finally, some concluding remarks are drawn in Section 4.

2. METHODS

2.1. Image pre-processing.

Since the green channel component of color retinal images provides the best contrast and the most relevant clinical visual information [8], the green channel of these images designated by $I_G(\mathbf{x})$ is used as input to the proposed algorithm. No contrast normalization or enhancement is performed on the $I_G(\mathbf{x})$ image. If $I_G(\mathbf{x})$ has either a width or height smaller than 1000 pixels, it is proportionally resized using a bicubic interpolation, leading to a dimension of 1000 pixels in the smaller direction.

2.2. Scale-space definition

As referred in [9], the linearity of the structure depends on the observation scale. This is particularly relevant in the smaller and thinner retinal vessels that are usually more difficult to detect and extract, indicating the need for a scale-space approach. In this paper a set of Gaussian filters $G(\mathbf{x}, \sigma)$ with the corresponding $\sigma = \{2.8, 2.9, 3\}$ are used to define each scale. At each scale σ the following operation was used,

$$L(\mathbf{x}, \sigma) = I_G(\mathbf{x}) * G(\mathbf{x}, \sigma), \quad (1)$$

Here, the two-dimensional Gaussian $G(\mathbf{x}, \sigma)$ is defined as, $G(\mathbf{x}, \sigma) = \frac{1}{(2\pi\sigma^2)} \exp -\frac{|\mathbf{x}|^2}{2\sigma^2}$. The proposed algorithm is ap-

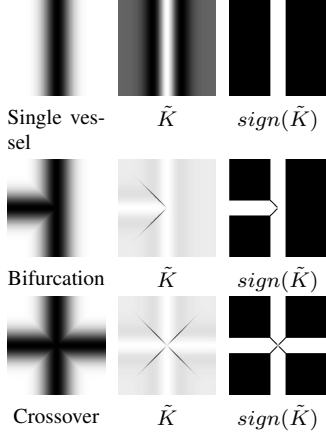


Fig. 2: $\tilde{K}(\mathbf{x}, \sigma)$ for a synthetic single vessel, vessels bifurcation and vessels crossover, created with a standard deviation of 2. $sign(\cdot)$ stands for the signum function.

plied at each scale σ , and the results are then combined to form the final vessel centerline image.

2.3. Vessel detector

By considering the image $L(\mathbf{x}, \sigma)$ as an intensity surface, Wang and Brady proposed a corner detection algorithm based on the measurement of the surface curvature [10]. Furthermore, if the corner points are also edge points, then the corner detector is defined as,

$$K(\mathbf{x}, \sigma) = (\nabla^2 L(\mathbf{x}, \sigma))^2 - c|\nabla L(\mathbf{x}, \sigma)|^2. \quad (2)$$

$K(\mathbf{x}, \sigma)$ enhances regions where a rapid change in the edge direction occurs. The parameter c defines how edge-phobic is $K(\mathbf{x}, \sigma)$, being set to $c = 1$ in our implementation. To enable a better response of the vessel structures relative to its surroundings, the square of the first term in (2) is removed, resulting in,

$$\tilde{K}(\mathbf{x}, \sigma) = \nabla^2 L(\mathbf{x}, \sigma) - c|\nabla L(\mathbf{x}, \sigma)|^2. \quad (3)$$

Equation (3) reveals to be a good vessel detector, because it allows a good preservation of elongated structures. Moreover provides a good discrimination between vessel and non-vessel structures. Figure 2 shows the application in the three most common vessel situations, namely, a single vessel, vessel bifurcation and vessels crossover. There can be observed that $\tilde{K}(\mathbf{x}, \sigma)$ exhibits a higher response in the center of the vessels. Figure 4 a) shows $\tilde{K}(\mathbf{x}, \sigma)$ for a retinal fundus image.

2.4. Vessel enhancement

As proposed in [11] it is possible to enhance the vasculature structure in retinal images by using a technique designated by

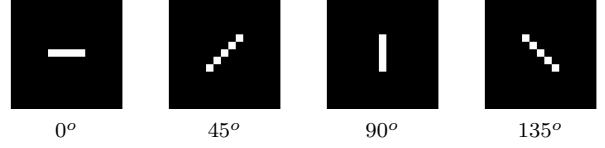


Fig. 3: Some binary Φ filters for the $0^\circ, 45^\circ, 90^\circ$ and 135° directions with $l = 5$.

matched filtering (MF). This method uses a spatial model of the object to be recognized. In this case the cross-section of the vessels can be modelled by a Gaussian function. Therefore, a Gaussian-shaped filter can be used to “match” the vessels. The Gaussian MF kernel can be defined as,

$$m(\mathbf{x}) = -\exp(-x^2/2s^2), \quad \forall |y| \leq W/2, \quad (4)$$

where W is the length of the vessel segment that has the same orientation and s defines the spread of the vessel intensity profile [11]. For the vessels detection, the kernel is rotated to match all possible vessel orientations and the maximum response from the filter bank is registered. In order to further enhance the difference between vessels and non-vessels structures, a few modifications are incorporated to the initial MF algorithm. Instead of applying the matching filtering directly to the $I_G(\mathbf{x}, \sigma)$ image, it is applied to the defined vessel detector $\tilde{K}(\mathbf{x}, \sigma)$. Moreover, the used kernels were also modified. Instead of applying a Gaussian MF kernel, a set of $2D$ binary filters composed by a white line and designated here by Φ are used. Since the vessels can have any orientation, h must be rotated to several angles θ . Furthermore, to achieve further effective enhancement, several line lengths designated by l must also be considered. Hence $\Phi \equiv \Phi(\mathbf{x}, l, \theta, d)$, where d is the corresponding filter size for each l (see Figure 3 as an example). After extensive testing, the following set of values were defined, $l = \{3, 5, 7, 9, 11\}$ with the respective filter size $d = \{[5 \times 5], [7 \times 7], [9 \times 9], [13 \times 13], [15 \times 15]\}$, and θ varied from 15° , from 0° to 165° in steps of 15° . The correlation between $\tilde{K}(\mathbf{x}, \sigma)$ and the kernel $\Phi(\mathbf{x}, l, \theta, d)$ can be defined as $\hat{R}(\tilde{K}(\mathbf{x}, \sigma), \Phi(\mathbf{x}, l, \theta, d))$. In order to obtain the maximum response of the considered filter bank, the following operation was applied,

$$C(\mathbf{x}, \sigma) = \max_{\forall \theta, l} \{\hat{R}(\tilde{K}(\mathbf{x}, \sigma), \Phi(\mathbf{x}, l, \theta, d))\}. \quad (5)$$

where $C(\mathbf{x}, \sigma)$ represents the maxima of the correlation of $\tilde{K}(\mathbf{x}, \sigma)$ with the filter $\Phi(\mathbf{x}, l, \theta, d)$ (represented in Figure 4 b)). The comparison of the images in Figure 4 shows that $C(\mathbf{x}, \sigma)$ offers a better distinction between vessels and non-vessels than $\tilde{K}(\mathbf{x}, \sigma)$. Furthermore, it is also observed that even the smaller and thinner vessels appear well contrasted in relation to its surroundings. These observations indicate that a simple thresholding could select the majority of the vessels structures.

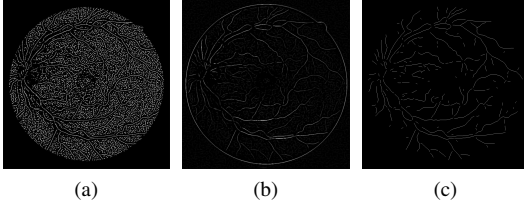


Fig. 4: a) Output of the vessel detector $\tilde{K}(\mathbf{x}, \sigma)$. b) Enhanced version of $\tilde{K}(\mathbf{x}, \sigma)$, $C(\mathbf{x}, \sigma)$. c) Thresholded version of $C(\mathbf{x}, \sigma)$, $C_\alpha(\mathbf{x}, \sigma)$

2.5. Vessels thresholding

In order to perform the selection of the vessels in $C(\mathbf{x}, \sigma)$ a threshold α must be defined. α shall be dynamically computed since each $C(\mathbf{x}, \sigma)$ image requires a different threshold. This is achieved based on the fact that only the highest intensity pixels in $C(\mathbf{x}, \sigma)$ corresponds to the vessel centerlines. Hence, all $C(\mathbf{x}, \sigma)$ values larger than zero are selected, and sorted in an ascending order in a vector \mathbf{v} . The value of \mathbf{v} that is smaller than the $\beta\%$ maxima values of \mathbf{v} is selected as the threshold α . After extensive testing β was set to 7%. All the pixels in $C(\mathbf{x}, \sigma)$ smaller than α are set to 0. In order to refine the results, a morphological “thinning” operation followed by the removal of all the regions smaller than 12 pixels is applied. The image that results from this thresholding operation followed by the morphological refinement is designated by $C_\alpha(\mathbf{x}, \sigma)$. An example is represented in Figure 4 c).

2.6. Directional vessel centerline detector

Although, the described procedure reveals a good performance, it is obvious from the observation of Figure 4 c) that some connections between vessels are missing, particularly in bifurcations and crossovers regions. To overcome this problem, it is determined the directional vessel centerline, ie, the vessel centerline for a specific direction. Subsequently, this information can be used to establish the missing crossovers and bifurcations in the $C_\alpha(\mathbf{x}, \sigma)$ image. Since the vessels can occur in any direction, it is necessary to select a reduced number of orientations that shall be analysed. As indicated in [5] the set $\phi = \{0^\circ, 45^\circ, 90^\circ, 135^\circ\}$ are an interesting trade-off between accuracy and computation time. Hence, the initial image $L(\mathbf{x}, \sigma)$ is processed with a set of directional filters capable of detecting retinal vessels centerlines in the ϕ orientations. The kernels used in this work are the first-order derivative filters, known as the difference of offset Gaussians filters (DoOG filters), which have revealed good immunity to noise due to their larger size [5, 12]. The particular kernel used for detecting vertical centerline candidates is the row gradient filter, given by,

$$\begin{bmatrix} -1 & -2 & 0 & 2 & 1 \\ -2 & -4 & 0 & 4 & 2 \\ -1 & -2 & 0 & 2 & 1 \end{bmatrix}.$$

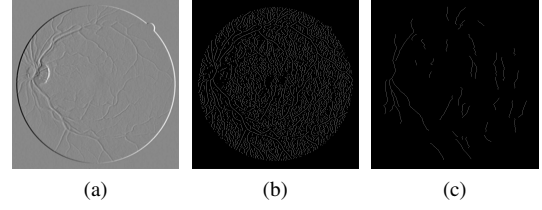


Fig. 5: a) Result of the DoOG filter in the vertical direction, $D_{90^\circ}(\mathbf{x}, \sigma)$. b) Vessel centerlines at the vertical orientation, $M_{90^\circ}(\mathbf{x}, \sigma)$. c) Vertical vessel centerlines after the algorithm of Figure 6.

The other three kernels are just rotated versions of this filter. The Convolution of $L(\mathbf{x}, \sigma)$ with these DoOG kernels measures the gradient component in a specific direction, generating the directional images $D_\phi(\mathbf{x}, \sigma)$ with $\phi = \{0^\circ, 45^\circ, 90^\circ, 135^\circ\}$ (see Figure 5 a)). Each one of these four directional images $D_\phi(\mathbf{x}, \sigma)$ are searched in a pixel-by-pixel basis for specific combinations of signs on the expected direction of the vessel cross section. Hence, and considering the $D_{90^\circ}(\mathbf{x}, \sigma)$ image as an example, the pixel position $\mathbf{x} = (x, y)$ is considered as a vessel candidate if the neighborhood pixels in the normal direction have the signal combinations that result in $M_{90^\circ}(\mathbf{x}, \sigma)$ equal to 1,

$$M_{90^\circ}(\mathbf{x}, \sigma) = \begin{cases} 1, & \text{if } \begin{cases} D_{90^\circ}(x, y - 2, \sigma) > 0 \wedge \\ D_{90^\circ}(x, y - 1, \sigma) > 0 \wedge \\ D_{90^\circ}(x, y + 2, \sigma) < 0 \wedge \\ D_{90^\circ}(x, y + 1, \sigma) < 0 \end{cases} \\ 0, & \text{otherwise} \end{cases} \quad (6)$$

$M_{90^\circ}(\mathbf{x})$ are the vessels centerlines candidates in the vertical orientation, as represented in Figure 5 b). This procedure can be easily extend to the remaining orientations, creating $M_{0^\circ}(\mathbf{x})$, $M_{45^\circ}(\mathbf{x})$ and $M_{135^\circ}(\mathbf{x})$. In order to refine the results, a morphological “thinning” operation is applied to all $M_\phi(\mathbf{x}, \sigma)$ with $\phi = \{0^\circ, 45^\circ, 90^\circ, 135^\circ\}$.

2.7. Final vessel centerline calculation

As previously mentioned, some bifurcations and crossovers in C_α are missing. To overcome this problem, it was determined the directional vessel centerlines $M_\phi(\mathbf{x}, \sigma)$ with $\phi = \{0^\circ, 45^\circ, 90^\circ, 135^\circ\}$. Since we have four different orientations, each $M_\phi(\mathbf{x}, \sigma)$ must be individually combined with $C_\alpha(\mathbf{x}, \sigma)$. Furthermore, it is also observed from Figure 4 c) and Figure 5 b) that the images C_α and $M_i(\mathbf{x}, \sigma)$ are formed by individual regions, where each region represents a possible vessel centerline candidate. Based on these considerations, the algorithm of Figure 6 was implemented (see Figure 5 c) for the 90° degrees case). The final vessel centerline image at scale σ designated by $S(\mathbf{x}, \sigma)$ is created by the union of all $M_\phi(\mathbf{x}, \sigma)$ and $C_\alpha(\mathbf{x}, \sigma)$.

The final vessel centerline image for the image $I_G(\mathbf{x}, \sigma)$

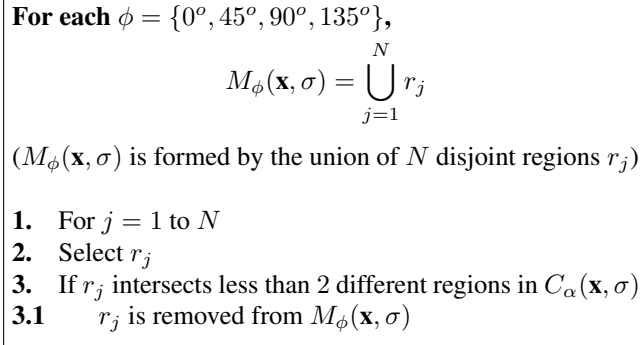


Fig. 6: Bifurcations and crossovers closing algorithm.

is given by,

$$F(\mathbf{x}) = \bigcup_{\sigma} S(\mathbf{x}, \sigma). \quad (7)$$

In Figure 7 some qualitative results are shown for the proposed algorithm.

3. RESULTS

An automatic system for the detection of the vessels centerline in retinal fundus images has been proposed. To evaluate the proposed algorithm, two publicly available datasets were used, namely the DRIVE dataset [13], composed of 40 images, and the STARE dataset [14], composed of 20 images. In both datasets only the vessels segmentation groundtruth images are available. The performance evaluation will use the segmentation groundtruth to evaluate the detected vessel centerlines which is somehow a limitation. Furthermore, as referred in [3], quantitative measures of segmentation are dominated by the performance on wide vessels, simply because wide vessels have more pixels. These evaluation limitations will be overcome with two different performance evaluation techniques. The first technique uses a (1-Precision) versus Recall curve proposed in [3]. The second evaluation method is based on the so called Estimated True Positive versus Estimated False Positive rates curve. The first evaluation method relies on the fact that an ideal vessel extraction should “match” a thinned version of the manual segmentation. This is not always the case and may induce an evaluation error. Instead, the second evaluation method relies on the fact that the number of pixels in an ideal vessel centerline extraction should be similar to the thinned version of the vessels segmentation groundtruth. The method reliability is based on the selection of the threshold value α , which is defined by the value of β . Hence, β was increased in steps of variable width to analyse its influence on the vessels centerline detection performance. The following values $\{35, 25, 15, 9, 7, 5, 3, 1\}$ were tested for β .

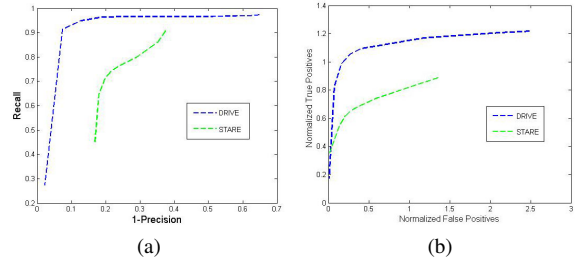


Fig. 8: Performance curves for the proposed method. a) (1-Precision) versus Recall curve. b) Estimated True Positive versus Estimated False Positive rates curve.

3.1. (1-Precision) versus Recall curve

For any retinal image, we can determine the number of true positive, false positive, and false negative vessel centerlines extracted for any β value. These values are defined by using a comparison against a “thinned” version of the groundtruth segmentations, as in [3]. A true positive is defined as any detected point within two pixels of the thinned groundtruth segmentation. False negatives are counted as the number of points in the thinned groundtruth segmentation not within two pixels of a detected centerline point. The tolerance of two pixels was suggested in [3] to account for localization errors in both the thinned manual segmentation and in the centerline peak location. Recall is the true-positive detection rate, and (1-Precision) is defined as the number of false positives divided by the total number of detections. For each β the Recall and (1-Precision) is determined for each image, and then averaged for all the images in each dataset (see Figure 8 a)). In both datasets, the best results were achieved to a $\beta = 7\%$. For the DRIVE dataset the Recall and (1-Precision) were respectively of 0.96 and 0.19 with an Area Under the Curve (AUC) of 87.28%. For the STARE dataset the Recall and (1-Precision) were respectively 0.74 and 0.22 with an AUC of 73.67%.

3.2. Estimated True Positive versus Estimated False Positive rates curve

For each retinal image, the number of true positives and false positives was determined as explained in the following. A true positive is any detected point within the groundtruth segmentation. A false positive is any detected point outside the groundtruth segmentation. Next, a “thinned” version of the groundtruth segmentations is determined, designated by G_t . For any retinal image the Estimated True Positive rate, is defined by $\frac{\text{true positive}}{\text{number of } G_t \text{ pixels}}$. The Estimated False Positive rate, is defined by $\frac{\text{false positive}}{\text{number of } G_t \text{ pixels}}$. For each β the Estimated True Positive and Estimated False Negative rates are determined for each image, and then averaged for all the images in each dataset (see Figure 8 b)). In both datasets, the best results were achieved for $\beta = 7\%$. For the DRIVE

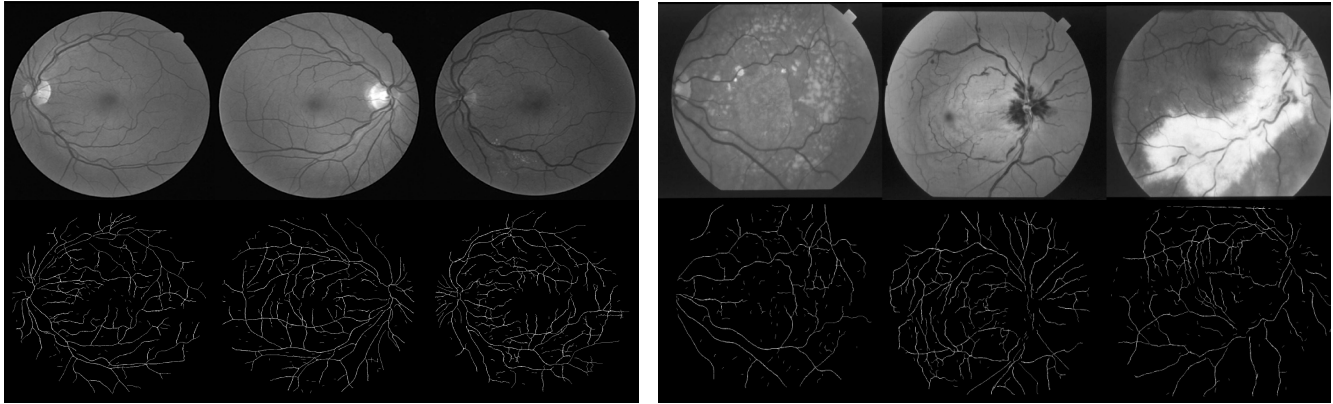


Fig. 7: Vessel centerlines detection examples using some images from the DRIVE dataset (first three images) and STARE dataset (last three images).

dataset the Estimated True Positive and the Estimated False Positive rates were respectively 1.05 and 0.27 with an AUC of 96.75%. For the STARE dataset the Estimated True Positive and the Estimated False Positive rates were respectively 0.65 and 0.27 with an AUC of 66.31%. The worst performance of the described method with the STARE dataset results of the poor images quality with many pathological signs. The Estimated True and False positive rates may assume values larger than one because they assume a different groundtruth as reference.

4. DISCUSSION

In this paper, a new method to the detection of retinal vessels centerline is proposed. Very few works were presented that specifically deals with vessels centerline extraction, which restrain any results comparison with other methods. Despite the evaluation limitations given by the manual segmentations, the achieved results, suggests that the proposed method is very effective in vessel centerlines extraction, providing a good basis for the vessels segmentation and vascular tortuosity evaluation. This was confirmed by visual inspection as in Figure 7 where some examples for the proposed method are shown.

REFERENCES

- [1] Conor Heneghan, John Flynn, Michael O'Keefe, et al., "Characterization of changes in blood vessel width and tortuosity in retinopathy of prematurity using image analysis," *Medical Image Analysis*, vol. 6, no. 4, pp. 407 – 429, 2002.
- [2] Jaydeep De, Huiqi Li, and Li Cheng, "Tracing retinal vessel trees by transductive inference," *BMC Bioinformatics*, vol. 15, no. 1, pp. 20, 2014.
- [3] M. Sofka and C.V. Stewart, "Retinal vessel centerline extraction using multiscale matched filters, confidence and edge measures," *Medical Imaging, IEEE Transactions on*, vol. 25, no. 12, pp. 1531–1546, 2006.
- [4] M. M. Fraz, S. A. Barman, P. Remagnino, et al., "An approach to localize the retinal blood vessels using bit planes and centerline detection," *Comput. Methods Prog. Biomed.*, vol. 108, no. 2, pp. 600–616, 2012.
- [5] A.M. Mendonca and A. Campilho, "Segmentation of retinal blood vessels by combining the detection of centerlines and morphological reconstruction," *Medical Imaging, IEEE Transactions on*, vol. 25, no. 9, pp. 1200–1213, 2006.
- [6] William E. Hart, Michael Goldbaum, Paul Kube, et al., "Measurement and classification of retinal vascular tortuosity," *International Journal of Medical Informatics*, vol. 53, pp. 239–252, 1999.
- [7] F. Zana and J.-C. Klein, "Segmentation of vessel-like patterns using mathematical morphology and curvature evaluation," *Image Processing, IEEE Transactions on*, vol. 10, no. 7, pp. 1010–1019, Jul 2001.
- [8] R.J. Winder, P.J. Morrow, I.N. McRitchie, et al., "Algorithms for digital image processing in diabetic retinopathy," *Computerized Medical Imaging and Graphics*, vol. 33, no. 8, pp. 608 – 622, 2009.
- [9] H. E. Bennink, H. C. Van Assen, G. J. Streekstra, et al., "A novel 3d multi-scale liness filter for vessel detection," 2007, MICCAI'07, pp. 436–443.
- [10] Han Wang and Michael Brady, "Real-time corner detection algorithm for motion estimation," *Image and Vision Computing*, vol. 13, no. 9, pp. 695 – 703, 1995.
- [11] S. Chaudhuri, S. Chatterjee, N. Katz, M. Nelson, and M. Goldbaum, "Detection of blood vessels in retinal images using two-dimensional matched filters," *Medical Imaging, IEEE Transactions on*, vol. 8, no. 3, pp. 263–269, 1989.
- [12] T. S. Yoo, G. D. Stetten, and B. Lorensen, *Basic image processing and linear operators, in Insight into Images*.
- [13] J. Staal, M.D. Abramoff, M. Niemeijer, et al., "Ridge-based vessel segmentation in color images of the retina," *Medical Imaging, IEEE Transactions on*, vol. 23, no. 4, pp. 501–509, 2004.
- [14] "Stare project website clemson university," Available from: <<http://www.parl.clemson.edu/~ahoover/stare/index.html>>.